Evaluation of load-carrying capacity of a semi-submersible platform subjected to accidental ice impacts

Zhaolong Yu & Jørgen Amdahl

Centre for Autonomous Marine Operations and Systems (AMOS), Norwegian University of Science and Technology (NTNU), Norway

Department of Marine Technology, Norwegian University of Science and Technology (NTNU), Norway

Sveinung Løset

Sustainable Arctic Marine and Coastal Technology (SAMCoT), Norwegian University of Science and Technology (NTNU), Trondheim, Norway

ABSTRACT: Floating glacial ice features of various sizes pose great threats to the structural integrity of offshore structures in arctic regions. Potential collisions with large icebergs should generally be avoided through proper ice management, but smaller glacial ice features such as bergy bits or growlers (with a characteristic water line < 15 m) may be overlooked by radar in high sea states, and are likely to hit the platform accidentally. This paper evaluates the load carrying capacity of a semi-submersible platform to accidental ice impacts. The shared energy approach is adopted as done in ship collision analysis, assuming collision scenarios with rigid platform-deformable ice on the one hand, and rigid ice-deformable structures on the other hand. Both ice and the platform should deform and dissipate energy under the same force level. For structural analysis, non-linear finite element code LS-DYNA is used. An alternative approach is the simplified analytical method, which allows for fast and reasonable prediction of structural damage. Simplified expressions for stiffened panels under ice pressure patch loading are introduced. The resulting resistance curves compare reasonably with LS-DYNA simulations.

1 INTRODUCTION

For ships and offshore structures serving in the arctic regions, potential threat from floating glacial ice impacts is a big concern. Glacial ice features of various sizes driven by environmental loads such as waves, currents and winds are likely to hit the structure. For safety considerations, it is crucial to understand the response of structures subjected accidental ice collisions and to properly design structures against such abnormal actions.

For now, it is still challenging to accurately assess the risk of platforms exposed to glacial ice impacts, the associated impact energy and the consequences of such actions. One reason is owing to the complicated interaction between ice and environmental loads, e.g. waves, currents and winds. Particular interests related to ice impacts would be to study the hydrodynamic interactions when ice approaches the platform, and how this interaction influences the final impact energy (Sayeed et al., 2017). In addition, ice, as a material, has complicated mechanical properties. It is difficult to model properly the ice behavior in an integrated impact analysis. A simple way of representing ice is to use a pressure-area relationship.

For assessing the impact energy, a rational procedure would require probabilistic analysis of a large number of impact events over a long period in the studied region and select a proper value of exceedance probability. The NORSOK-N003 (2007) recommends the design impact energy based on an annual exceedance probability 10^{-4} in the Accidental Limit States (ALS) and 10^{-2} in the Ultimate Limit States (ULS). This is applicable for ice impacts according to ISO-19906 (2010). In the ALS conditions, damage to the structure is allowed provided that it does not lead to progressive collapse of the platform and the structure maintains sufficient residual capacity before it can be repaired. This is in contrast to the Ultimate Limit States (ULS) conditions, where the structure should resist foreseeable ice loads with certain safety margins.

In order to gain deep insights of ice-platform impacts under environmental loads, the Norwegian Petroleum Safety Authority (PTIL) initiated a series of research projects to assess the platform capacity to resist accidental ice impacts. This paper is part of the work originating from the ST19 project (Lu et al., 2018), which evaluates the capacity of a semi-submersible against ice impacts. Small bergy bits or growlers are of major concern because they are not easily detected by radar in due time and are difficult to perform concurrent ice management operations. The shared energy approach is adopted as done in ship collision analysis, assuming collision scenarios of rigid platform-deformable ice and on the other hand, rigid ice-deformable structures. Both ice and the platform should deform and dissipate energy under the same force level. For structural analysis, non-linear finite element code LS-DYNA is used. An alternative

approach is the simplified analytical method, which allows for fast and reasonable prediction of structural damage. Simplified expressions for stiffened panels under ice pressure patch loading are introduced.

2. THE SHARED ENERGY APPROACH

In order to calculate the distribution of energy dissipation between ice and the structure, we will adopt the same principles as those used for ship collisions. The principle is sketched in Figure 1. The ship may represent ice feature in the present context. The force-deformation curve for the installation is established assuming the ship or ice to be rigid. Likewise, the force-deformation curve for the ship or ice is established assuming the installation to be rigid. The resulting damage is determined when the energy dissipation reaches the demand for energy dissipation, as determined by the external mechanics analysis.

It is noted that this approach does not take the coupling of interaction effects into account. For ship collisions, deformation of the ship increases the contact area and may hence increase the capacity of the installation resistance (Yu and Amdahl, 2018), as seen from the dashed line in Figure 1. Similarly, interaction effects exist for ice-structure collisions, but these are associated with significant uncertainties at present. The interaction effect is not included in the current analysis.

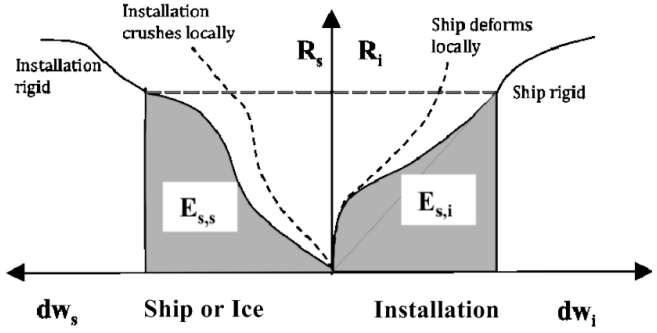

Figure 1. Dissipation of strain energy in the installation and ship/ice during impacts (DNV-RP-C204, 2010)

3. THE ICE PRESSURE-AREA RELATIONSHIP IN ACCIDENTAL LIMIT STATES

A pressure area relationship is often used to represent ice strength $p = CA^{ex}$, where p is the ice pressure, A is the nominal contact area, and C and ex are coefficients for calibration. In the ULS design according to ISO-19906 (2010), a pressure area relationship of $p = 7.4A^{-0.7}\ (\text{MPa})$ is derived using probabilistic analysis of pond inlet tests, where a mean pressure plus three times standard deviation is adopted. This is generally used for ULS considerations, but is too conservative for the energy absorption consideration. In the accidental limit states, the peak pressures are not of major concern because the struck structure is allowed to deform provided that it does not lead to progressive collapse of the platform and the structure maintains sufficient residual capacity before it can be repaired. The mean pressure level and the mean energy absorption capacity will be of major interest. The ice load model $F=CA^{(1+ex)}$ with C=3.2 MPa and ex=-0.1 accounts for physically plausible energy absorption capacity of freshwater ice during ice feature structure interaction process (refer to Figure 2). The same ice-load model is used by the International Association of Classification Societies (IACS) for calculating energy dissipation in ice for PC3 ice class vessels.

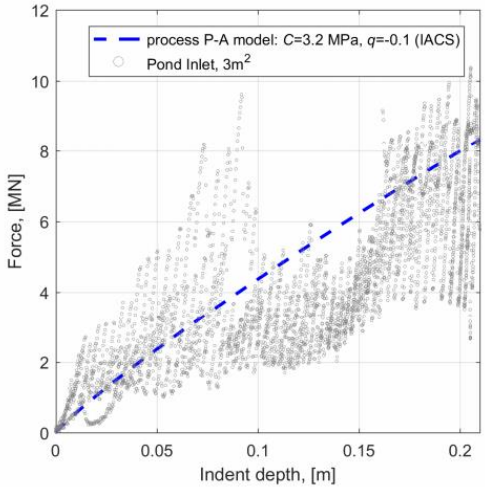

Figure 2. The IACS load-disp curve and the experimental curve (Lu et al., 2018)

4. MODEL DESCRIPTION

4.1 The column FE model of the submersible platform

The column leg of the Midgard structure is studied. It was modelled by Tavakoli and Amdahl (2010) for assessment of structural strength against supply vessel collisions. Only the front part of one leg was modelled. The overall dimension of the column FE-model is 17200 mm x 308750 mm x 6100 mm (w x h x d). The finite element models of the column is shown in Figure 3. The column outer shell is in the range of 16-18 mm. The vertical stiffeners used in the column are HP 320x12, HP 300x11 and HP 240x10. These stiffeners were modelled as L-bars with dimensions 320 x 50 x 40 x 12 (mm), 300 x 50 x 50 x 11 (mm) and 240 x 40 x 30 x10 (mm). This gives nearly the same height, width and the cross sectional area as the HPs. The column model was meshed using approximately 245,000 4-noded shell elements. The general element size is 120 mm.

Numerical simulations were carried out by using explicit NLFEM software LS-DYNA 971. The four-node Belytschko-Lin-Tsay shell element with reduced integration was used with 5 integration points through the thickness. Hourglass stiffness is added using the stiffness based form (option 4 in LS-DYNA). The rear side, the top and the bottom of the column are constrained in all degrees of freedom

(translation in direction of x-, y- and z-axis and rotation around x-, y- and z-axis).The rigid ice model is given a prescribed motion velocity of 3 m/s, and any strain rate effect is not taken into account. Two kinds of contacts are defined in this analysis, which are the self-contact and master-slave contact. For the rigid ice-column collision, the master-slave contact is used with the column being the slave part. Self-contacts are defined for the column model to detect possible contacts due to deformation. A static friction coefficient of 0.3 was used for all the contacts.

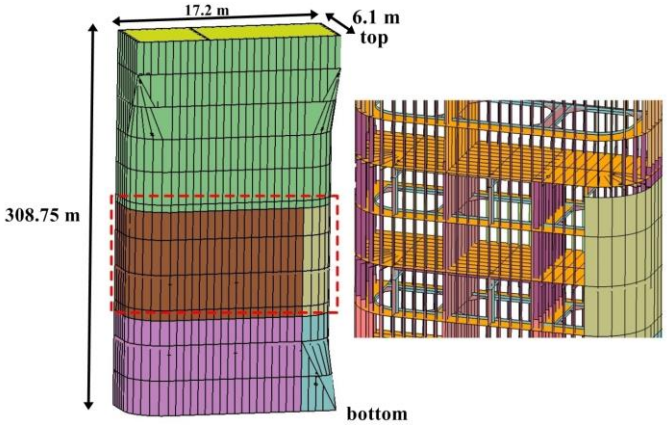

Figure 3. The finite element model of the structure column.

4.2 The rigid ice model

It is considered that the global ice geometry influences the mass distribution, moment of inertia, etc., and therefore influences the absorbed impact energy through external dynamics, but how to dissipate the energy obtained from external dynamics will be influenced by local ice geometries; see, e.g. Kim et al. (2019). However, it is not the focus of the present paper to address the influence of local ice geometries. Local sharp geometry should be avoided because they will be crushed anyway in reality. Without loss of generality, the ice shape is assumed to be an ellipsoid with the long axis of 15 m and a short axis of 10.4 m as shown in Figure 4.

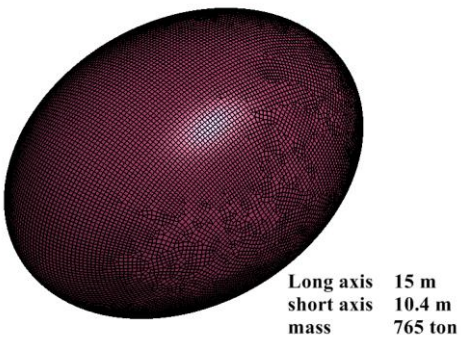

Figure 4. The ice model

4.3 Material and fracture modelling

Two kinds of steel material grades are used for the structure materials, and the material properties are shown in Table 1. The outer shell material is with a yield stress of 420 MPa, while the stiffeners are modelled with a 355 MPa yield stress steel. The BWH (Bressan-Williams-Hill) instability criterion is used to model fracture in the ice collision simulation. The BWH criterion considers that fracture occurs at the onset of local necking instability neglecting the post-necking regime, and this is conservative for structural safety.

Table 1. Properties of the steel material

Steel for	Plate	HP stiffener
Young moduls (MPa)	2.07×10^5	2.07×10^5
Yield stress(MPa)	420	355
Poisson ratio	0.3	0.3
Power law K (MPa)	860	780
Power law n	0.16	0.22
$\varepsilon_{plateau}$	0.0	0.0

4.4 Collision scenario

The potential collision locations depend upon the size and draft of the structure and the ice. In addition, wave-induced relative motions of the structure and the ice increase the vertical extension of the collision exposed area. From the probabilistic analysis of motions in waves and current, potential collision locations varies from 5.5 m above the waterline to 10 m below the waterline (Lu et al., 2018). From the point of view of structural arrangements, several representative impact locations are selected on the column as shown in Figure 5, including the column corner, bulkhead, cruciform, and stiffened panels of column front. The collision scenarios are shown in Figure 6.

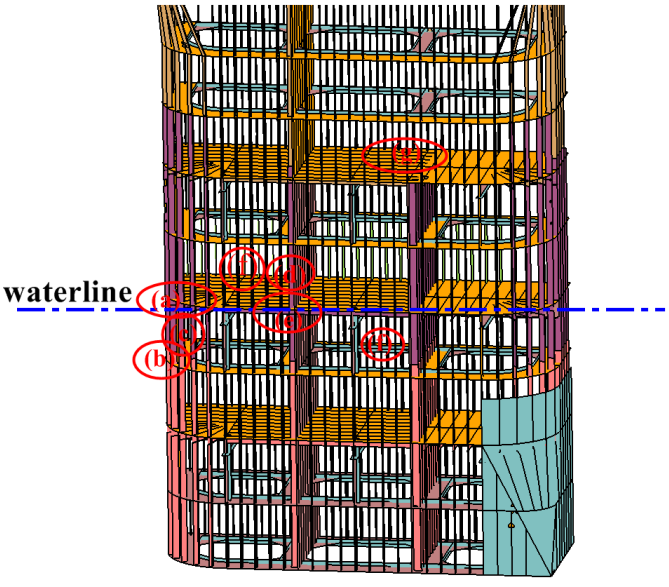

(a): column corner with the stiffened deck
(b): column corner with the unstiffened transverse ring frame
(c): middle column corner (d): stiffened bulkhead
(e): cruciform (f, g): confined stiffened panel

Figure 5. The collision locations

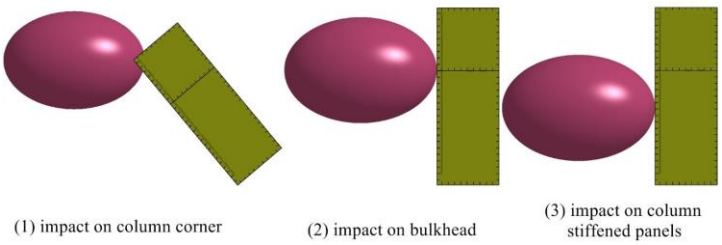

Figure 6. The collision scenarios

5. NON-LINEAR FEM SIMULATION RESULTS

Figure 7 plots on the right-hand side, the structural collision resistance on seven different locations from LS-DYNA simulations assuming rigid ice, while on the left-hand side, the ice crushing resistance assuming rigid structures is plotted. Under the same force level, both the ice and the structure should deform and absorb energy in accordance with the resistance curves, and the area below the curves are the corresponding energy that is dissipated in ice and the structure, respectively.

From Figure 7, the column bulkhead and cruciform represent hard points of the structure, and are capable of crushing ice significantly. Below a certain force level (around 6 MN for bulkhead and 12 MN for the cruciform), all the deformation goes to the ice. The column stiffened panels have similar force level with that of the ice, and therefore both the ice and the stiffened panels deform and absorb around 50% of the total energy. The resist force of the column corner is much lower than the column side, but it is interesting to observe that the ice crushing force on the corner defined by SAMS (Simulator for Arctic Marine Structures) is also lower than the ice crushing force from the column side. This makes the strengths of ice and structure on the column corner very close, and both objects will deform to absorb the energy.

Figure 8 summarizes the energy absorption with increasing crushing distances. From probabilistic analysis under considered wave spectrum, an energy dissipation of 7.5 MJ is considered critical in the given environmental conditions; see Lu et al. (2018). If all the energy 7.5 MJ goes to the structure, this will result in a crushing distance of 0.4-0.7 m. In reality, the total energy should be shared by both ice crushing and structural deformations, and the resulting deformation of the structures will be less. Considering shared energy in ice and the structure, the permanent deformation of the structures with a total energy dissipation of 7.5 MJ is summarized in Table 2.

It is found that given a total energy of 7.5 MJ, both the ice and the column structure should deform and dissipate part of the energy. The crushing distance can vary from 0.25 m to 0.55 m depending on the collision locations. As initial outer shell rupture generally occurs at 0.6 m-0.9 m, the structure is considered safe from compartment flooding for the given collision energy. It is noted that the markers (small vertical lines) on Figure 7 represent initial fracture of the outer shell when one element is eroded. There is still considerable capacity from one element erosion to large outer shell opening.

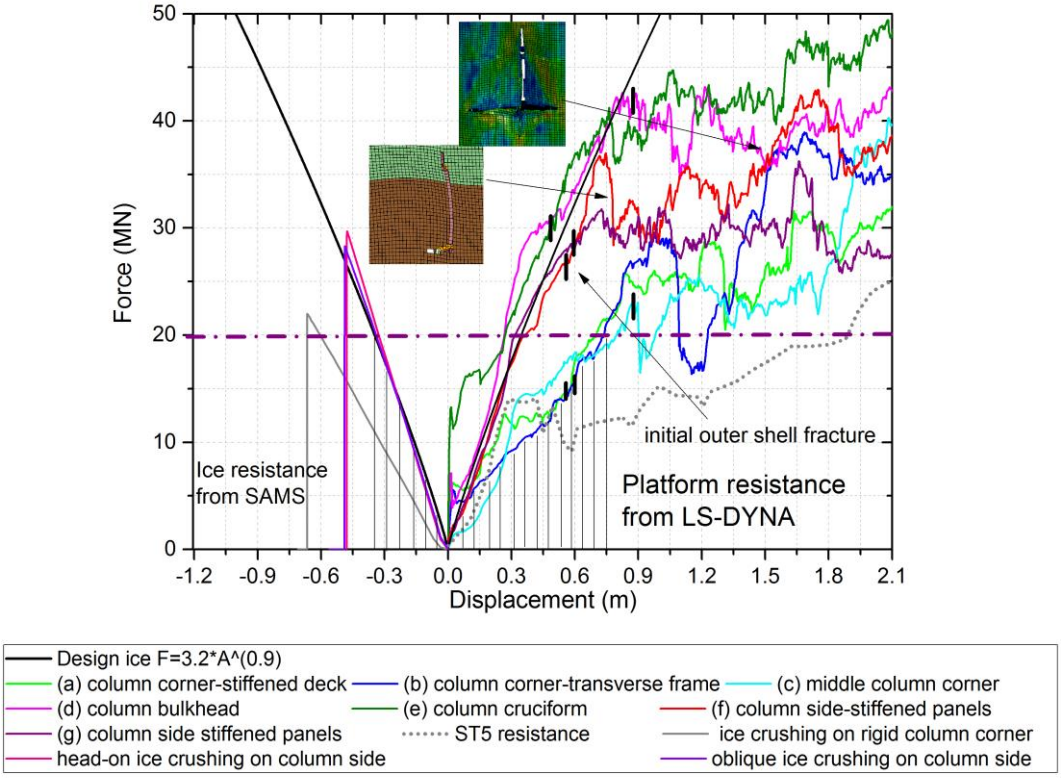

Figure 7. Collision resistance during ice-structure impacts

Table 2. Ice and structural deformation with a total energy of 7.5 MJ

	Location corner (a)	Location corner (b)	Location corner (c)	Location (d)	Location (e)	Location (f)	Location (g)
Ice crushing	0.41 m	0.42 m	0.48 m	0.37 m	0.33 m	0.33 m	0.36 m
Structural displacement	0.51 m	0.55 m	0.50 m	0.29 m	0.27 m	0.38 m	0.36 m
Energy in ice	2.5 MJ	2.7 MJ	3.55 MJ	4.1 MJ	3.2 MJ	3.2 MJ	3.75 MJ
Energy in structure	5.0 MJ	4.8 MJ	3.95 MJ	3.4 MJ	4.3 MJ	4.3 MJ	3.75 MJ

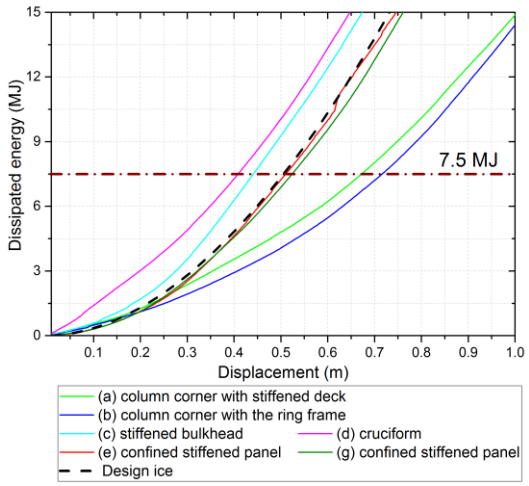

Figure 8. Energy absorption in the ice-structure collisions

6. SIMPLIFIED ANALYTICAL METHODS FOR BEAM RESPONSE OF A STIFFENED PANEL STRIP UNDER POINT AND PATCH LOADING

Nonlinear finite element simulations are capable of predicting structural responses with very good accuracy. However, numerical simulations require significant modelling efforts and computational costs. An alternative approach to that is the simplified analytical method, which gives fast and reasonable predictions. Examples of simplified analytical methods are Amdahl (1983) and Yamada and Pedersen (2008) for bow collisions, Wierzbicki and Suh (1988) for indentation of tubes, and Jones et al. (1970) for plastic response of clamped plates. Such simplified methods are especially useful in the design stage and can be utilized in rules and standards.

6.1 Simplified formulations

The assessment of structural resistance for a stiffened panel strip with associated plate flange undergoing finite deformations is carried out in accordance with the recommended practice DNV GL-RP-C204 (Updated, unreleased version 2018). The formulas is based on the work by Yu et al. (2018). The total resistance is considered to consist of a bending contribution and a membrane contribution for finite deflections as illustrated in Figure 9.

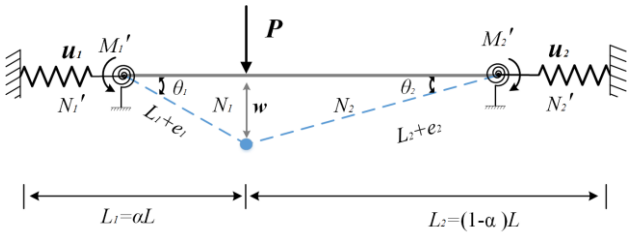

Figure 9. Model for the assessment of structural resistance for stiffener with plate flange during large deflection and finite axial stiffness. *k* is stiffness against inward motion.

The resistance is given by the following set of equations:

$$\frac{P}{P_0}=\frac{M}{M_p}+\frac{N\delta}{\beta M_p};\quad \beta=\begin{cases}1 & \text{free rotation}\\ 2 & \text{fixed rotation}\end{cases} \tag{1}$$

where, the resistance to plastic bending, P_0, plastic bending moment, M_p, and plastic axial force, N_p, of the stiffener with associated plate flange are given by Eq. (2).

$$\begin{aligned} P_0 &= \beta M_p\left(\frac{1}{\alpha L}+\frac{1}{(1-\alpha)L}\right)\\ M_p &= \sigma_y\left(\frac{1}{2}A_w h_w + A_t h_w\right)\\ N_p &= \sigma_y A_e \end{aligned} \tag{2}$$

The development of the membrane force is determined by:

$$\begin{aligned} \frac{N}{N_p} &= \left(\frac{16}{\beta^2 c}\left(\frac{A_w}{A_e}\right)^2-\left(2\frac{A_p}{A_e}-1\right)\right)\left[\exp\left(-\frac{\beta c}{4}\frac{A_e}{A_w}\frac{\delta}{h_w}\right)-1\right]\\ &\quad +\frac{4}{\beta}\frac{A_w}{A_e}\frac{\delta}{h_w};\quad \left(stage\,1,2,3:\frac{N}{N_p}<1\right)\\ \frac{N}{N_p} &= 1;\quad stage\,4 \end{aligned} \tag{3}$$

where c is the non-dimensional axial stiffness given by:

$$c=\frac{k_{eq}h_w^{\,2}}{\alpha(1-\alpha)LN_p} \tag{4}$$

The development of the bending moment is calculated from:

$$\frac{M}{M_p}=1;\quad \left(stage\,1:\frac{N}{N_p}\le\frac{2A_p}{A_e}-1\right)$$

$$\frac{M}{M_p}=1-\frac{1}{4}\frac{1}{1+2\dfrac{A_f}{A_w}}\left(\frac{A_e}{A_w}\right)^2\left\{\left(\frac{N}{N_p}-\left(\frac{2A_p}{A_e}-1\right)\right\}^2;\quad \left(stage\,2:\frac{2A_p}{A_e}-1<\frac{N}{N_p}<1-\frac{2A_f}{A_e}\right)\right. \tag{5}$$

$$\frac{M}{M_p}=\frac{\dfrac{A_e}{A_w}}{1+2\dfrac{A_f}{A_w}}\left(1-\frac{N}{N_p}\right);\quad \left(stage\,3:1-\frac{2A_f}{A_e}\le\frac{N}{N_p}<1\right)$$

$$M=0;\quad stage\,4$$

The resistance of the stiffened plate strip depends upon the non-dimensional axial flexibility $c(\mathrm{k})$, the relative size of the plate flange vs stiffener area ($A_p/A_s \ge 1$) and the size of the top flange versus the web area (A_f/A_w), as shown in Figure 10. In the present case, it will be reasonably representative to assume that $c(\mathrm{k})$ is large (i.e. clamped conditions).

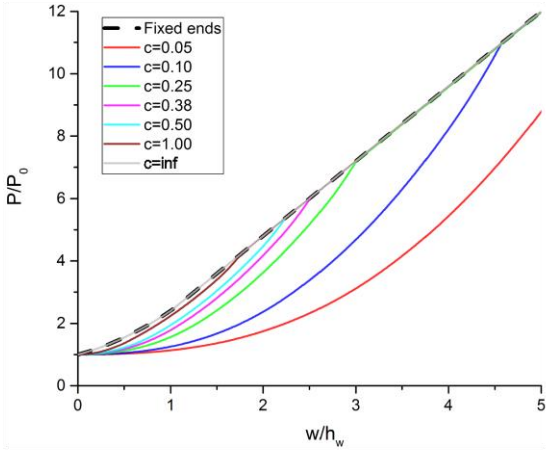

Figure. 10. Resistance-displacement curves for stiffened panels given different translational stiffness (Yu et al., 2018)

For a stiffened panel strip under pressure patch loading (refer Figure 11), the pressure p is given by,

$$p=\frac{P}{WB\left(1-\dfrac{B}{2L}\right)} \tag{6}$$

W is the width of the plate flange.

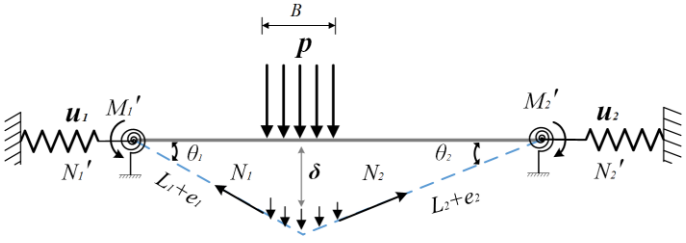

Figure 11. Beam deformation under patch loading.

6.2 Comparison with LS-DYNA simulations

Extensive validation of the above formulations have been carried out in Yu et al. (2018) by comparison with experiments and numerical simulations. More verification here is on patch loaded stiffened panel strips.

A stiffened panel strip is modelled in accordance with dimensions of the column stiffened panel as shown in Figure 12. The bottom plate dimension is 2.9 m×0.625 m×18 mm. The stiffener web is 0.32 m×12 mm while the stiffener flange is 0.05m×40 mm. The steel material in Table 1 with a yield strength of 420 MPa is used. The model is discretized with fine meshes, and the mesh size is typically 50 mm. The ends of the stiffened panel strip is fixed in all degrees of freedom.

The force-displacement curves with different patch length is shown in Figure 13. It shows that under patch loading with different patch lengths, the model is capable of predicting the resistance curves with good accuracy. The shear effect may degrade the initial bending capacity of the beam. This however does not influence the structural capacity for energy absorption in the accidental limit states. The stiffened strip deformation is shown in Figure 12 (right), and significant web buckling can be observed. The effect of web buckling and strain hardening tends to counteract each other, and the influence on the accuracy of the simplified model is limited.

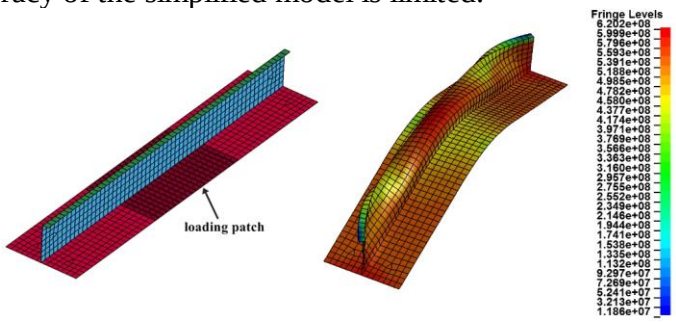

Figure 12. (Left) a stiffened panel strip model from the column (Right) deformation of the stiffened beam strip with a patch length of 1.0 m.

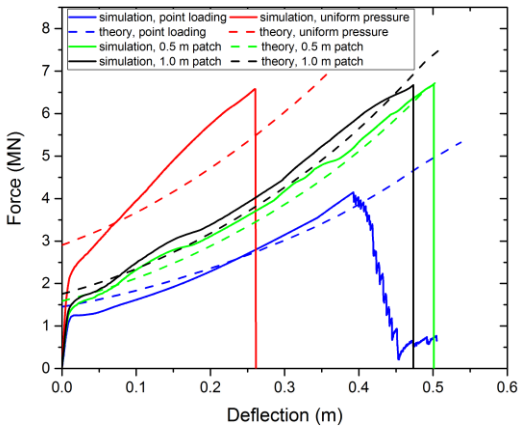

Figure. 13. Beam deformation under patch loading

CONCLUSIONS

This paper evaluates the load-carrying capacity of a semi-submersible platform subjected to ice impacts. The shared energy approach is adopted as done for ship collisions assuming rigid ice-deformable platform and rigid platform-deformable ice, respectively.

The structural resistance was obtained from non-linear finite element simulations and simplified analytical methods.

Results showed that the strengths of ice and the platform fall in the shared energy regime, where both ice and the platform structure will deform considerably. Bulkheads and cruciform represent hard points of the platform. For an energy dissipation of 7.5 MJ from probability analysis, no fracture occurs on the platform. The platform preserves sufficient margins for even higher energy level impact.

For assessing platform resistance, a simplified model was proposed for beam response of stiffened panels under point and patch ice loading. Results showed that boundary axial stiffness influence significantly the platform resistance-deformation curves.

REFERENCES

AMDAHL, J. 1983. Energy absorption in ship-platform impacts. Doctoral Thesis, Norwegian Institute of technology.

DNV-RP-C204 2010. Recommended practice DNV-RP-C204. *DET NORSKE VERITAS*.

ISO-19906 2010. arctic offshore structures standard.

JONES, N., URAN, T. O. & TEKIN, S. A. 1970. The dynamic plastic behavior of fully clamped rectangular plates. *International Journal of Solids and Structures,* 6**,** 1499-1512.

KIM, E., YU, Z., AMDAHL, J. & LØSET, S. 2019. Uncertainty quantification in the ice-induced local damage assessment of a hull section. *the 25th International Conference on Port and Ocean Engineering under Arctic Conditions (POAC 2019)*.

LU, W., YU, Z., VAN DEN BERG, M., LUBBAD, R., AMDAHL, J., LØSET, S. & KIM, E. 2018. Assessment of Structural Damage due to Glacial Ice Impact. *PTIL-Konstruksjonssikkerhet i Nordområdene, Petroleumstilsynet, Stavanger*.

NORSOK-N003 2007. Action and action effects.

SAYEED, T., COLBOURNE, B., QUINTON, B., MOLYNEUX, D., PENG, H. & SPENCER, D. 2017. A review of iceberg and bergy bit hydrodynamic interaction with offshore structures. *Cold Regions Science and Technology,* 135**,** 34-50.

TAVAKOLI, M. T. & AMDAHL, J. 2010. Analysis of collision between Midgard platform and 8000 tonnes displacement ship

WIERZBICKI, T. & SUH, M. 1988. Indentation of tubes under combined loading. *International Journal of Mechanical Sciences,* 30**,** 229-248.

YAMADA, Y. & PEDERSEN, P. 2008. A benchmark study of procedures for analysis of axial crushing of bulbous bows. *Marine Structures,* 21**,** 257-293.

YU, Z. & AMDAHL, J. 2018. Analysis and design of offshore tubular members against ship impacts. *Marine Structures,* 58**,** 109-135.

YU, Z., AMDAHL, J. & SHA, Y. 2018. Large inelastic deformation resistance of stiffened panels subjected to lateral loading. *Marine Structures,* 59**,** 342-367.